CellPress

Cancer Cell
Article

Genomic Profiling of Hepatocellular Adenomas Reveals Recurrent FRK-Activating Mutations and the Mechanisms of Malignant Transformation

Camilla Pilati,[1,2] Eric Letouzé,[3] Jean-Charles Nault,[1,2] Sandrine Imbeaud,[1,2] Anaïs Boulai,[1,2] Julien Calderaro,[1,2,4] Karine Poussin,[1,2] Andrea Franconi,[1,2] Gabrielle Couchy,[1,2] Guillaume Morcrette,[1,2] Maxime Mallet,[1,2] Saïd Taouji,[5] Charles Balabaud,[5] Benoit Terris,[6] Frédéric Canal,[7] Valérie Paradis,[8] Jean-Yves Scoazec,[9] Anne de Muret,[10] Catherine Guettier,[11,12] Paulette Bioulac-Sage,[5,13] Eric Chevet,[5] Fabien Calvo,[14] and Jessica Zucman-Rossi[1,2,15,*]

[1]INSERM, UMR-1162, Génomique fonctionnelle des tumeurs solides, IUH, 75010 Paris, France
[2]Labex Immuno-oncology, Université Paris Descartes, Sorbonne Paris Cité, Faculté de Médecine, 75006 Paris, France
[3]Programme Cartes d'Identité des Tumeurs, Ligue Nationale Contre le Cancer, 75013 Paris, France
[4]Department of Pathology, Assistance Publique-Hôpitaux de Paris, CHU Henri Mondor, 94000 Créteil, France
[5]INSERM, UMR-1053, Université de Bordeaux, 33076 Bordeaux, France
[6]Department of Pathology, Assistance Publique-Hôpitaux de Paris, Cochin Hospital, 75014 Paris, France
[7]Institut Cochin, INSERM U1016, Université Paris Descartes, CNRS UMR8104, 75014 Paris, France
[8]Department of Pathology, Assistance Publique-Hôpitaux de Paris, Beaujon Hospital, Université Paris Diderot, 92210 Clichy, France
[9]Department of Pathology, Edouard Herriot Hospital, 69437 Lyon, France
[10]Department of Hepatogastroenterology, Centre Hospitalier de Tours, Trousseau Hospital, 37044 Tours, France
[11]Department of Pathology, Assistance Publique-Hôpitaux de Paris, CHU Bicêtre, 94275 Le Kremlin-Bicêtre, France
[12]Department of Pathology, Assistance Publique-Hôpitaux de Paris, CHU Paul Brousse, 94800 Villejuif, France
[13]Department of Pathology, CHU de Bordeaux, Pellegrin Hospital, 33076, Bordeaux, France
[14]Institut National du Cancer, INCa, 92513 Boulogne, France
[15]Assistance Publique-Hôpitaux de Paris, Hôpital Européen Georges-Pompidou, 75015 Paris, France
*Correspondence: jessica.zucman-rossi@inserm.fr
http://dx.doi.org/10.1016/j.ccr.2014.03.005

SUMMARY

Hepatocellular adenomas (HCA) are benign liver tumors predominantly developed in women using oral contraceptives. Here, exome sequencing identified recurrent somatic FRK mutations that induce constitutive kinase activity, STAT3 activation, and cell proliferation sensitive to Src inhibitors. We also found uncommon recurrent mutations activating JAK1, gp130, or β-catenin. Chromosome copy number and methylation profiling revealed patterns that correlated with specific gene mutations and tumor phenotypes. Finally, integrative analysis of HCAs transformed to hepatocellular carcinoma revealed β-catenin mutation as an early alteration and *TERT* promoter mutations as associated with the last step of the adenoma-carcinoma transition. In conclusion, we identified the genomic diversity in benign hepatocyte proliferation, several therapeutic targets, and the key genomic determinants of the adenoma-carcinoma transformation sequence.

INTRODUCTION

Hepatocellular adenomas (HCA) are rare benign tumors mainly developed in women after 2 years of oral contraceptive use (Rooks et al., 1979). HCA are also related to other risk factors (obesity, vascular diseases, and androgen and alcohol intake) or to different genetic diseases (McCune-Albright syndrome, glycogen storage disease type 1a, and maturity-onset diabetes

Significance

Malignant transformation of benign adenoma into malignant carcinoma is frequently observed in several epithelial tumor types. Adenoma-carcinoma transition is crucial for the patient prognosis; however, little is known on the molecular mechanisms involved. Here, we performed an integrated genomic analysis of hepatocellular adenomas (HCA). Among several gene mutations, we identified recurrent somatic mutation activating FRK, a Src-like kinase. FRK-activating mutations induce STAT3 activation and cell proliferation targetable by Src inhibitors. Focusing on malignant transformation of HCA in hepatocellular carcinoma, we identified *CTNNB1* and *TERT* promoter mutations as early and late genomic events, respectively, involved in adenoma-carcinoma transition. In conclusion, we propose to introduce targeted therapies and an identification of adenomas with the highest risk of malignant transformation in clinical practice.

of the young type 3 diabetes caused by HNF1A germline mutation) (Calderaro et al., 2013; Nault et al., 2013a). Bleeding and malignant transformation to hepatocellular carcinoma (HCC) can occur as severe complications observed, respectively, in 30%–50% and 5% of the cases. In the past 10 years, we identified four major molecular subgroups of HCA defined by (1) mutations inactivating HNF1A (H-HCA, 35% of the HCA) (Bacq et al., 2003; Bluteau et al., 2002; Jeannot et al., 2010), (2) activation of β-catenin by mutations in exon 3 (bHCA, 15%) (Chen et al., 2002), (3) inflammatory phenotype with STAT3 activation (IHCA, 50%) (Bioulac-Sage et al., 2009; Zucman-Rossi et al., 2006), and (4) the remaining unclassified tumors (UHCA, 10%) (Bioulac-Sage et al., 2009) (See Experimental Procedures for details on molecular group assessment.). Among bHCA, half displayed both inflammatory and β-catenin-activated phenotypes (bIHCA). Inflammatory adenomas (IHCA) are caused by *IL6ST* somatic mutation activating gp130 in 60% of the cases (Poussin et al., 2013; Rebouissou et al., 2009), whereas other IHCA are mutated for *STAT3* itself (Pilati et al., 2011) or *GNAS* (Nault et al., 2012), but in the remaining 30% of the cases no mutations were identified yet. This molecular classification is currently accepted in clinical practice using either immunohistochemical markers (Bioulac-Sage et al., 2007, 2009) or in radiology at magnetic resonance imaging (Laumonier et al., 2008), and it has dramatically improved the diagnosis and prognostic assessment of HCA.

The aim of this work was to better characterize genomic alterations causing benign proliferation of hepatocytes and their malignant transformation to improve the molecular classification and identify oncogenic events useful to propose a more personalized care of HCA patients in the future.

RESULTS

Spectrum of Mutations Identified by Exome Sequencing

We analyzed a series of 250 tumors from 195 patients including 223 classical HCAs without any suspicion of malignancy, 18 borderline lesions between HCA and HCC (HCA/HCC), and nine cases of HCCs derived from HCA malignant transformation (HCC on HCA); clinical, histological, and molecular features are described in Tables S1 and S2 (available online). Among them, whole-exome sequencing was performed using a SureSelect Enrichment System (Agilent Technologies) and a HiSeq instrument (Illumina) (see Supplemental Experimental Procedures). Tumor and corresponding nontumor DNA was sequenced in 35 classical HCAs developed in 25 patients, including nine H-HCAs, 11 IHCAs, four bHCAs, and four bIHCAs mutated in exon 3 of *CTNNB1*, and seven UHCAs (Table S3). One IHCA and one UHCA displayed a mutation of *CTNNB1* located in exon 7 and were reclassified as bIHCA and bHCA, respectively (see below). The average coverage of each base in the targeted regions was 70-fold (Figure S1). Somatic mutations were systematically verified using integrative genomics viewer inspection and/or Sanger sequencing (see Supplemental Experimental Procedures and Table S4). This strategy led to the validation of 508 somatic mutations in the 35 tumors; among them, 264 (52%) were predicted to have damaging consequences at the protein level, whereas 124 (24%) were silent and 120 (24%) were predicted to be benign functionally using PPH2 (Polyphen-2) software (Figure 1A). The mean number of predicted damaging mutations was 7.5 events per HCA tumor; it was not significantly variable in the different HCA molecular subgroups (Figure S1) but lower than that observed in hepatocellular carcinoma (41 events per HCC [Guichard et al., 2012], $p < 0.0001$). Analysis of the spectrum of nucleotide mutations identified a high frequency of transversions with a predominance of G>T changes that accumulated on nontranscribed strand in all subgroups (Figure 1B). This spectrum of nucleotide change was similar to that observed in the exome sequence of classical HCC (Guichard et al., 2012), suggesting that both benign and malignant hepatocyte proliferation could be promoted by exposure to genotoxic agents that still remain to be identified in dedicated epidemiological studies.

Exome sequencing of the 35 classical HCAs identified recurrent mutations in nine different genes (Figure 1C). *CTNNB1*, *IL6ST*, *HNF1A*, and *FRK* were mutated in at least three HCA tumors, and they were validated in the whole series of 250 tumors (Figure 1D; Table S5; Figure S1). *SLCO1B3*, *KPNA4*, *ALK*, *DDX11*, and *KIAA1109* were mutated in only two tumors representing seven different HCAs. Because these gene mutations were not associated with specific phenotype, they were not further screened in the entire series of tumors. Overall, a mutation occurring in a gene recurrently mutated was identified in 205/250 (82%) of the HCA cases (Figure 1D). *HNF1A* and *CTNNB1* mutations were identified in all H-HCA and 33/35 bHCAs, respectively. Twenty-eight of 41 bIHCAs harbored mutations in *CTNNB1* and *IL6ST*. Inflammatory adenomas displayed mutations in the known drivers *IL6ST*, *STAT3*, and *GNAS*, but also novel mutations in *FRK* and *JAK1*.

Among our whole series, the presence of two or more nodules synchronously developed in the same patient was observed in 49% of the cases (Table S1). Exome sequencing of 10 pairs of HCAs developed in 10 patients revealed in nine of these ten cases that the two tumors belonged to the same molecular subgroup: in four cases both adenomas were mutated for *HNF1A*, in three cases both tumors were IHCA (*IL6ST* mutated and *FRK* in one pair each, *IL6ST* and *JAK1* in the last pair), in one case both tumors were *CTNNB1* mutated, and in the last patient both tumors remained unclassified (Table S6). In the remaining patient one HCA was inflammatory, whereas the second HCA was unclassified. However, in nine of the ten cases, no common nucleotide mutations were identified among the paired adenomas, suggesting an independent development of the tumors. In the only pair with common mutations, the two H-HCA tumors shared one *HNF1A* mutation (Q211P) and a somatic substitution in *HDAC4* (T1055R). Interestingly, the two nodules were joined and they accumulated different private alterations, including inactivation of the second allele of *HNF1A* (Table S6), suggesting that HNF1A monoallelic inactivation added to an HDAC4 mutation could be an early event in the history of this case.

FRK-Activating Mutations in IHCA

Among the 35 HCAs analyzed by exome sequencing, three different IHCAs exhibited a somatic mutation of the fyn-related kinase (FRK, also known as RAK). FRK is a non-receptor-tyrosine kinase related to the Src kinase family, first proposed as a tumor suppressor in breast cancer cells (Yim et al., 2009). In the whole series of 250 tumors, we identified a heterozygous somatic *FRK* mutation in eight additional IHCAs and one bIHCA

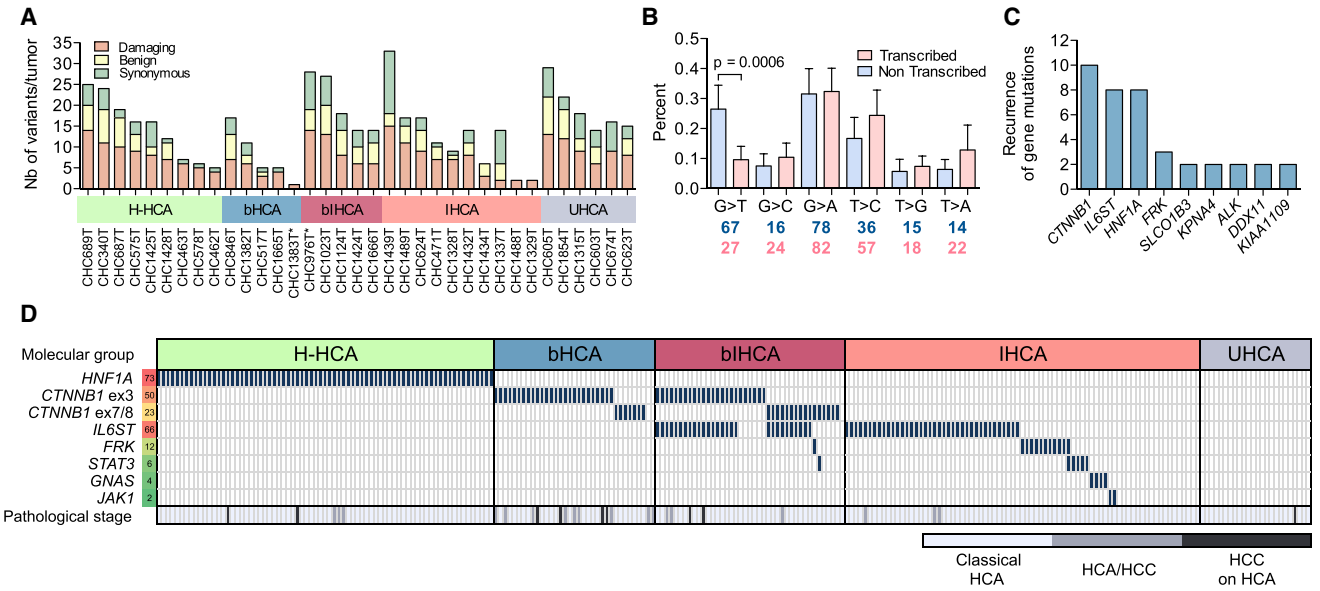

Figure 1. Profiles of Mutations in HCA Identified by Exome Sequencing

(A) Distribution of the 508 somatic mutations in the 35 HCA tumors according to their functional consequences (damaging, benign, and synonymous) predicted by PPH2 (Polyphen-2). Asterisk (*) indicates HCA with *CTNNB1* exon 7 mutations.

(B) Type of mutations on the transcribed (pink) and the nontranscribed (blue) strands for the 455 nucleotide substitutions identified in exome sequencing of 35 HCAs (means with 95% CI; two-tailed Mann-Whitney test).

(C) Genes recurrently mutated in classical HCA with damaging consequences.

(D) Somatic mutations (blue boxes) identified in 250 tumors (columns) among seven classical HCA-altered genes (rows). The number of events per gene is indicated on the left.

See also Figure S1 and Tables S1, S2, S3, S4, S5, and S6.

(Figure 1D). All FRK mutations were located in the tyrosine kinase catalytic domain, and two hot spots were identified: an amino acid substitution located at codon 346 in four cases and eight small in-frame deletions/insertions at codons V378 and/or F379 in eight cases (Figure 2A; Table S5). In one case (1130), we identified two nucleotide mutations that led to amino acid substitutions at codons 346 and 350 carried by the same allele. Overall, *FRK* was the second most frequently mutated gene in our series of IHCA (12/118, 10%).

No recurrent FRK mutations are currently described in tumors. In HCA, the mutation pattern including two hot spots and in-frame deletion/insertion suggested that FRK mutations could have gain of function. To test this hypothesis, we reproduced six different mutants identified in IHCA by site-directed mutagenesis in a *FRK* full-length cDNA. All the tested FRK mutants induced a strong acute inflammatory response in hepatocellular cell lines with overexpression of two inflammatory target genes, *SOCS3* and *CRP*, independently of interleukin-6 (IL-6) exposure (Figure 2B; Figures S2A–S2C). This inflammatory response was proportional to the amount of transfected mutants (Spearman's $r = 0.89$, $p = 0.01$; Figure S2B). FRK mutants induced the activation of STAT3 as assessed by its phosphorylation at Y705 and its nuclear translocation, whereas wild-type FRK had no effect on STAT3 phosphorylation and localization (Figures 2C and 2D). We further showed that VF and FK FRK mutant exhibited an increased kinase activity compared with the wild-type FRK, affecting both V_{max} and K_M (Figure 2E; Figure S2D). Next, we showed that four different Src inhibitors, namely, PP2, dasatinib, Src inhibitor 1, and Src inhibitor 5, were able to abrogate the constitutive kinase activity of FRK mutants (Figure 2F). Then, we selected dasatinib, an inhibitor currently used to cure leukemia patients (Talpaz et al., 2006). Treatment of Hep3B cells with dasatinib decreased the constitutive activity of FRK mutant in a dose-dependent manner, whereas it had no effect on IL-6-induced inflammation (Figure 2G).

Then, we stably transfected Ba/F3 cells, an interleukin-3 (IL-3)-dependent murine pro-B cell line, with wild-type or mutant FRK. In the presence of IL-3, cell proliferation was similar in all conditions (Figure S2E); in contrast, only Ba/F3 cells expressing the FRK mutants were able to grow upon IL-3 withdrawal (Figure 3A). We confirmed the proliferation advantage conferred by *FRK* overexpression in mice immortalized fibroblasts, NIH 3T3, cultured with a limiting amount of growth factors (Figure S2F). Also, in NIH 3T3, FRK mutants promoted cell foci formation without increasing cell migration or invasion (Figure 3B; Figures S2G and S2H). Interestingly, in Ba/F3 cells, IL-3-independent growth induced by FRK mutant was abrogated by dasatinib treatment (Figure 3C). Subcutaneous injection of Ba/F3 cells with stable expression of the VK FRK mutant in nude mice resulted in tumor growth. In contrast, Ba/F3 cells expressing wild-type *FRK* failed to promote tumor growth (Figure 3D). Allografted tumors showed nuclear and Y705-phosphorylated STAT3 (Figure 3E). Furthermore daily intraperitoneal injections of dasatinib (10 mg/kg/day) after subcutaneous tumor development and during 14 days led to a complete regression of the tumors (n = 9; Figures 3F and 3G; Figure S2I). Interestingly,

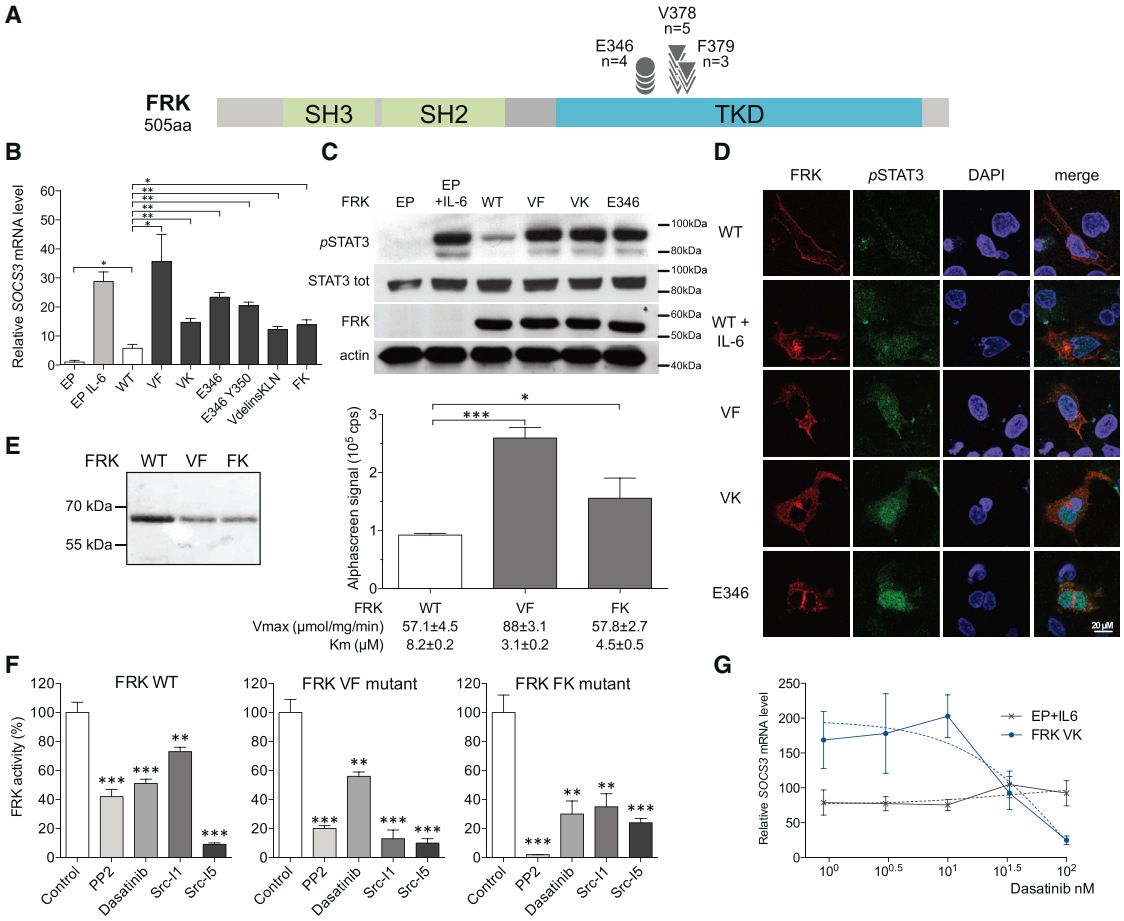

Figure 2. FRK Mutants Induce STAT3 Activation

(A) Spectrum of FRK mutations identified in 250 HCAs. Circles indicate amino acid (aa) substitutions and triangles are in-frame deletions. SH, Src homology domain; TKD, tyrosin kinase domain.

(B) Endogenous *SOCS3* mRNA expression of FRK mutants V378–F379 del (VF), V378–K380 delinsE (VK), E346G (E346), E346G Y350C (E346 Y350), V378 delinsKLN (VdelinsKLN), F379-K380 delinsL (FK), or control wild-type (WT) FRK (WT) and empty plasmid (EP) transfected in Hep3B. *$p < 0.05$; **$p < 0.01$; ***$p < 0.001$, two-tailed Student's t test.

(C) Expression of FRK, total STAT3, and Y705-phosphorylated STAT3 (pSTAT3) proteins in transfected Hep3B cells assessed by western blot.

(D) Subcellular localization of FRK and tyrosine phosphorylation of STAT3 at Y705 (pSTAT3) FRK and STAT3 proteins were analyzed by immunofluorescence, and images were obtained with a confocal microscope. Results are representative of three independent experiments.

(E) FRK proteins WT and mutants (VF and FK) were produced in *Escherichia coli*. The AlphaScreen method showed an increased kinase activity for FRK mutants with modified K_M and V_{max}. cps, counts per second.

(F) FRK kinase residual activity was measured in vitro by AlphaScreen method after treatment with four different Src inhibitors: PP2 (10 µM), dasatinib (10 µM), Src-I1 (10 µM), and Src-I5 (10 µM). *$p < 0.05$, **$p < 0.01$, ***$p < 0.001$, two-tailed Student's t test.

(G) Endogenous *SOCS3* mRNA expression of FRK VK mutant (blue) or empty vector treated with 100 ng/ml IL-6 (black) transfected in Hep3B exposed for 6 hr to increasing concentrations of dasatinib. Quantitative data are presented as mean ± SD.

See also Figure S2.

14 days after dasatinib withdrawal, tumors reappeared, confirming the oncogenic addiction of Ba/F3 cells to the FRK mutant tested (Figure 3G).

Mutations Activating JAK-STAT3 Pathway in IHCA

Exome sequencing of an inflammatory adenoma revealed a somatic missense mutation leading to S703I substitution in the JAK kinase *JAK1* previously identified in an acute lymphoblastic T cell leukemia (Zhang et al., 2012). Screening the entire sequence of *JAK1* in the whole series of 250 tumors revealed one additional IHCA with a heterozygous somatic JAK1 substitution A723D never described in tumors (Figure 1D; Figure 4A; Table S5). S703I and A723D mutants were different from the two classical V658 and R724 JAK1 substitutions known to activate the JAK-STAT pathway (Flex et al., 2008; Staerk et al., 2005). In Hep3B cells, we showed that expression of S703I or A723D was able to induce an inflammatory response and phosphorylation of STAT3 at Y705 (Figure 4B; Figures S3A and S3B). Moreover, the two JAK1 mutant proteins were phosphorylated at Y1022/1023, two regulatory tyrosines known to activate JAK1 when phosphorylated (Figure S3B). We also identified in an inflammatory HCA an unusual heterozygous somatic mutation in

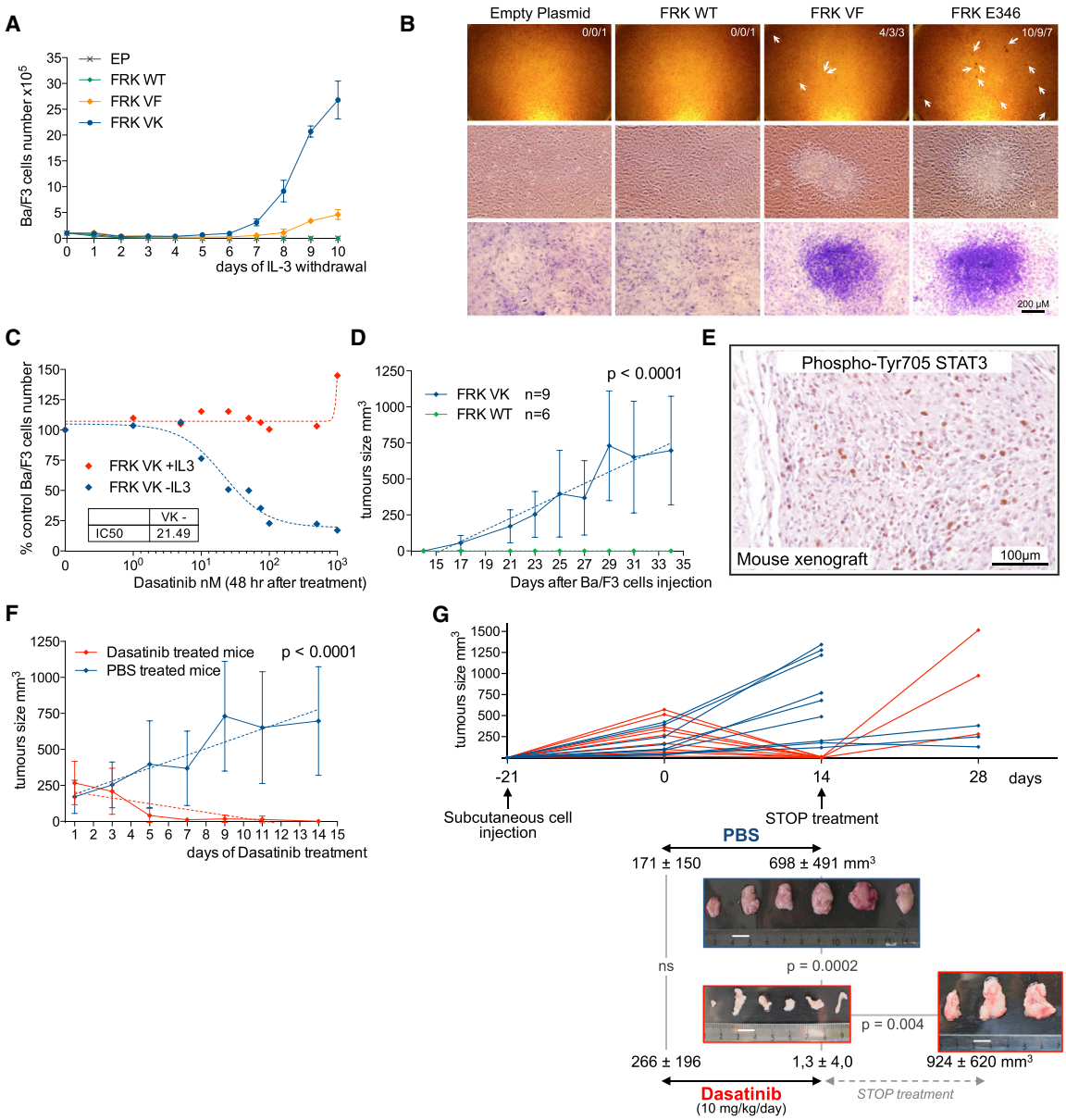

Figure 3. FRK Is a Targetable Activated Gene in HCA

(A) Growth of Ba/F3 cells stably transfected with FRK mutants (VF and VK) compared with FRK WT or EP after IL-3 withdrawal in triplicate experiments. Data shown indicate mean ± SD.

(B) Cell foci formation was observed in NIH 3T3 cells stably expressing FRK mutants VF (p = 0.003, t test) or E346 (p = 0.0009, t test) and not in cells transfected with WT FRK or EP. In white, the number of foci representative of three independent experiments.

(C) Ba/F3 cells transfected with FRK VK mutant treated (red) or untreated (blue) with 10 ng/ml IL-3 and exposed for 48 hr to increasing concentrations of dasatinib. The graph plots the proportion of treated cells relative to the transfected not-treated cells.

(D) Subcutaneous injection of 10^7 Ba/F3 cells with stable expression of VK FRK mutant (blue, n = 9) induced tumor growth in a BALB/c-nu/nu mouse model, whereas WT FRK (green, n = 6) failed (mean tumor volume, 95% CI, regression analysis).

(E) Representative staining of Y705 phosphorylation of STAT3 using immunohistochemistry in allograft tumors from VK FRK Ba/F3 cells 34 days after injection.

(F) Effect of dasatinib treatment on tumor size of mice allografted with Ba/F3 cells transfected with VK FRK mutant and treated daily with dasatinib (red, n = 9; 10 mg/kg/day) or with PBS as a control (blue, n = 9) (mean tumor volume, 95% CI, regression analysis).

(G) Effect of dasatinib withdrawal on allograft tumors from VK FRK Ba/F3 cells. Shown are the tumors of BALB/c-nu/nu mice treated daily with PBS (10 ml/kg, 14 days) as a control or with dasatinib (10 mg/kg/day, 14 days), and tumors treated with dasatinib during 14 days and left without treatment for 14 days (n = 3). Scale (white) bars, 10 mm.

the *IL6ST* gene, located at exon 10 and leading to the in-frame deletion of four amino acids (A418–F421) outside the mutation hot spot that we previously identified at the IL-6 binding site (Poussin et al., 2013; Rebouissou et al., 2009). Sequencing the entire coding sequence of *IL6ST* in the validation set of 250 tumors led to the identification of a similar A418–F421 deletion

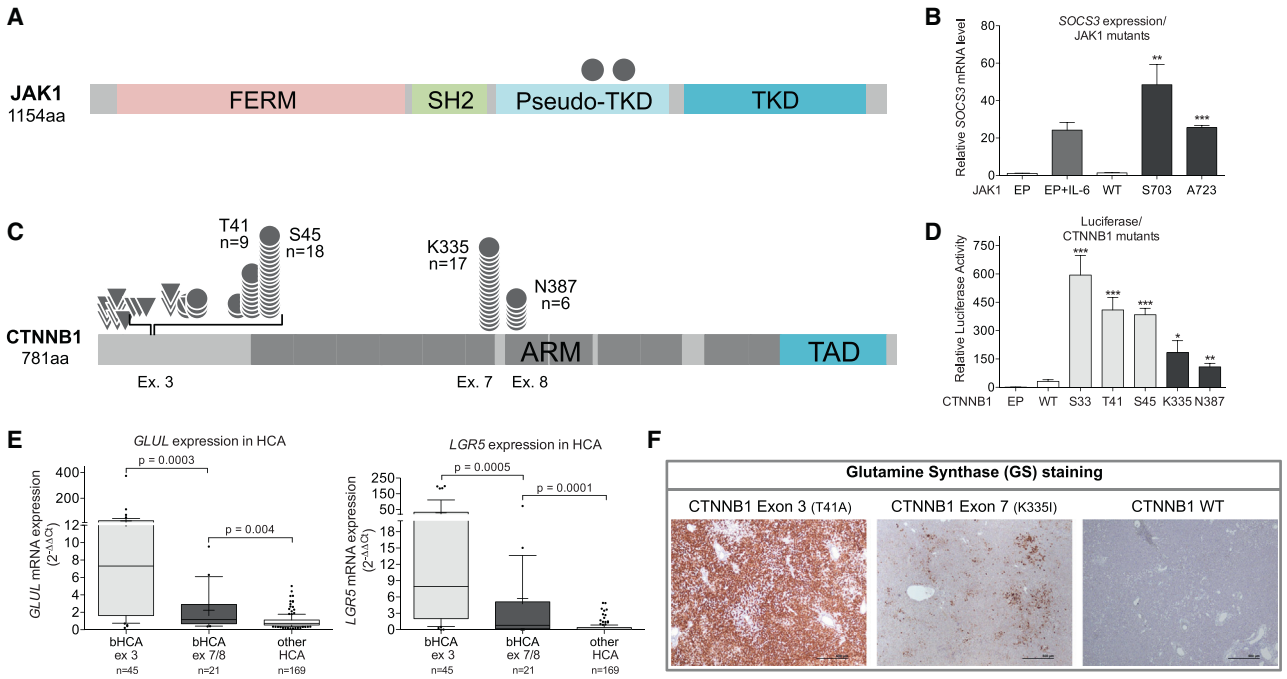

Figure 4. Identification of Uncommon Recurrent Gene Mutations in HCA and Functional Analysis

(A) Spectrum of *JAK1* mutations identified in 250 HCAs. Circles indicate aa substitutions.

(B) JAK1 mutants S703I (S703) and A723D (A723) or control WT JAK1 (WT) and EP were transfected in the Hep3B cell line. Graphs are quantitative (q)RT-PCR results showing the induction of endogenous *SOCS3* mRNA transcription measured after 6 hr of serum starvation and, when indicated, treated for 3 hr with 100 ng/ml IL-6 relative to unstimulated EP-transfected Hep3B cells. Data shown indicate mean ± SD. $^{**}p < 0.01$, $^{***}p < 0.001$, two-tailed Student's t test versus WT JAK1.

(C) Spectrum of *CTNNB1* mutations identified in 250 HCA. Circles indicate aa substitutions, and triangles are in-frame deletions. ARM, Armadillo repeat; TAD, transactivation domain.

(D) *CTNNB1* mutants S33Y (S33), T41A (T41), S45P (S45), K335I (K335), and N387K (N387) or control WT *CTNNB1* (WT) and empty plasmid (EP) were transfected in Huh7 cells expressing a *CTNNB1*-driven luciferase (TOP-FLASH) reporter construct. Shown is the luciferase activity determined from triplicate cotransfections relative to empty plasmid (EP). Data shown indicate mean ± SD. $^{*}p < 0.05$; $^{**}p < 0.01$; $^{***}p < 0.001$, two-tailed Student's t test versus WT *CTNNB1* with TOP-FLASH.

(E) Expression profiles of CTNNB1-exon 3 mutated HCA (n = 45), *CTNNB1*-exon 7- and -exon 8-mutated HCAs (n = 21) and *CTNNB1* WT HCA (n = 169). The graph shows the expression of *GLUL* (glutamine synthase) and *LGR5* by qRT-PCR relative to nontumor livers. Results are expressed as Tukey's boxplots; two-tailed Mann-Whitney test.

(F) Representative staining of glutamine synthase (GS) by immunohistochemistry in wild-type *CTNNB1* HCA, exon 7-mutated and exon 3-mutated bHCA. $^{*}p < 0.05$; $^{**}p < 0.01$; $^{***}p < 0.001$.

See also Figure S3.

in an additional IHCA (Figure S1). These mutations in exon 10 of *IL6ST* were exclusive from the classical mutation previously identified in exon 6. We further showed that this *IL6ST* mutant was able to constitutively activate gp130 in a cell culture model (Figure S3C). Finally, in the entire validation set of HCA, all the genes mutated in IHCA (*IL6ST, FRK, JAK1, STAT3*, and *GNAS*) were almost mutually exclusive; only one tumor showed mutations in both *FRK* and *STAT3* genes (Figure 1D).

Hot Spots of Mutations in *CTNNB1*

Exome sequencing in two HCAs revealed a mutation of *CTNNB1* located in exon 7 (K335I), outside *CTNNB1* exon 3 where the classical mutations activating β-catenin are usually located (Chen et al., 2002). Among the validation set of 250 tumors, we further identified two hot spots of substitutions at β-catenin codon 335 (K335I in 13 cases, K335T in four cases) and codon 387 located in exon 8 (N387K in six cases; Figure 4C). All HCAs with *CTNNB1* exon 7 and exon 8 mutations were previously considered as unclassified HCA (seven cases) or inflammatory adenoma (16 cases), and they were further classified for all analyses in the bHCA or bIHCA molecular subgroup. *CTNNB1* exon 7 and exon 8 mutations were mutually exclusive but also from mutations located at exon 3 and *HNF1A* mutations. We further showed that K335I and N387K mutants were able to activate β-catenin in a hepatocellular cell line, with a lower activity than the S33Y, T41A, and S45P mutants located within exon 3 (Figure 4D). Accordingly, most of the HCA tumors with exon 7 or exon 8 mutation exhibited a slight overexpression of glutamine synthase and *LGR5*, two classical genes activated by *CTNNB1* (Figure 4E). Immunohistochemical analyses of these cases revealed a faint patchy glutamine synthase expression without nuclear staining of β-catenin (Figure 4F). All these results showed that *CTNNB1* mutants at codons 335 and 387 weakly activate β-catenin in vivo in HCA.

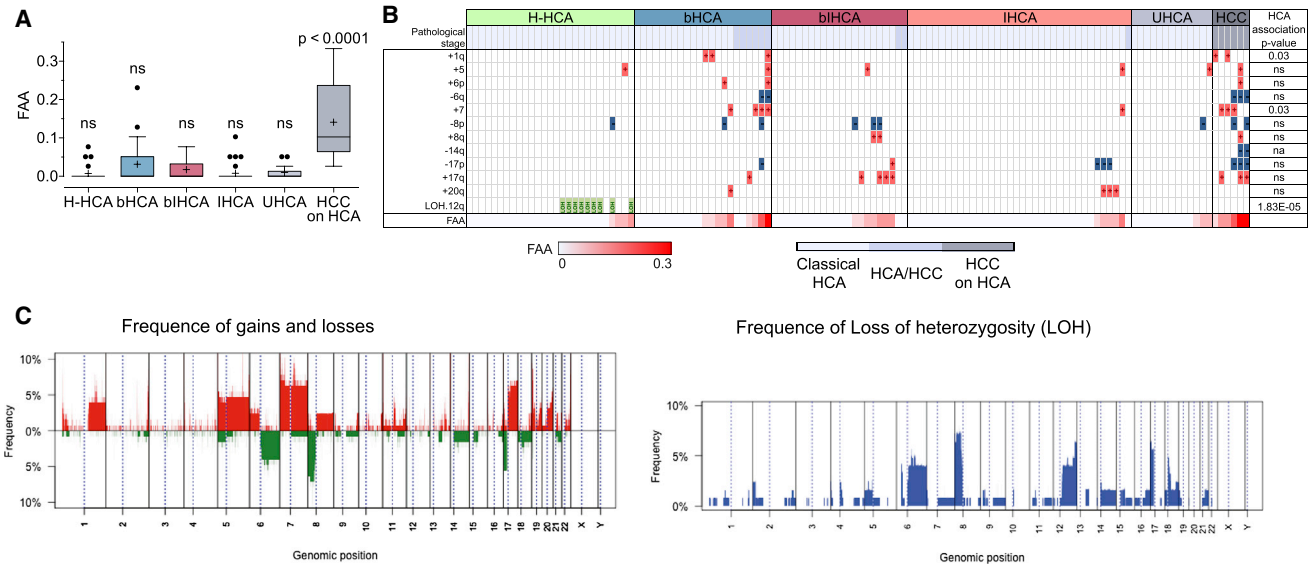

Figure 5. SNP Array Profiling of HCA Reveals Distinct Copy-Number Profiles Associated with Molecular Groups

(A) Distribution of genomic instability, defined as the FAA, in different molecular groups. Results are expressed as Tukey's boxplots; two-tailed Mann-Whitney test. ns, not significant

(B) Distribution of chromosome aberrations according to HCA molecular classification groups. LOH of chromosome 12q significantly associates with H-HCAs, whereas gains of 1q and of chromosome 7 associate with bHCA.

(C) Frequency of gains, deletions, and LOHs along the genome in a series of 111 classical HCAs, nine borderline lesions HCA/HCC, and six HCCs resulting from HCA malignant transformation.

See also Table S7.

Copy Number and Methylome Profiling

We profiled chromosome aberrations in 111 classical HCAs, nine borderline lesions HCA/HCC, and six HCC resulting from HCA malignant transformation. Although chromosomal instability, measured by the fraction of aberrant arms (FAA) score, was low and similar in the different molecular subgroups of classical adenomas (Figure 5A), we identified three recurrent events associated with specific molecular groups: bHCA showed more frequent gains of 1q ($p = 0.03$) and chromosome 7 ($p = 0.03$), whereas H-HCA presented frequent copy-neutral losses of heterozygosity (LOHs) at chromosome 12q, leading to a loss of the wild-type *HNF1A* gene and a duplication of the mutated allele ($p = 3.4 \times 10^{-6}$; Figures 5B and 5C; Table S7).

We then determined DNA methylation profiles in 50 hepatocellular adenomas and four normal liver samples using HumanMethylation450 arrays (Illumina). Consensus clustering identified two major clusters closely associated with the inflammatory phenotype (M1 and M2) or noninflammatory phenotypes (M3–M5). The partition in the five stable DNA methylation clusters (Figure 6A, M1–M5) was highly associated with specific molecular groups ($p = 3.4 \times 10^{-19}$, chi-square test; Figure 6B) and gene mutations. The M1 cluster included IHCA and mixed bIHCAs exclusively mutated in exon 7 or exon 8 of *CTNNB1*, whereas the M2 cluster included bIHCAs mutated in exon 3. Noninflammatory tumors were subdivided in clusters M3 including all H-HCA, M4 including most bHCA, and M5 including UHCA. Most DNA methylation changes occurred at CpG sites located outside CpG islands that displayed global hypomethylation in all tumor clusters compared with normal controls (Figure S4A). As described in HCC (Stefanska et al., 2011), hypomethylated regions formed genomic clusters, preferentially located at gene family loci (Figure S4B). Although the pattern of hypomethylation was similar in the five tumor clusters, the intensity of hypomethylation was significantly associated with methylation clusters ($p = 2.1 \times 10^{-4}$, ANOVA). Hypomethylation was weaker in clusters M1 and M2 (inflammatory HCA) and stronger in cluster M4 (bHCA), particularly in tumors that transformed into HCC (Figure 6C). There were few hypermethylated CpG sites, but we identified 640 genes specifically hypermethylated in cluster M3. Among them, 109 genes were hypermethylated and downregulated in H-HCA (significant overlap, $p = 2.4 \times 10^{-36}$, Fisher's exact test) (Table S8); they were significantly enriched in liver-specific genes ($p = 9.7 \times 10^{-6}$, hypergeometric test) (Figure 6D) and in genes known to be downregulated in liver cancer (Acevedo et al., 2008) ($p = 1.7 \times 10^{-14}$, hypergeometric test) (Table S9).

Alterations Involved in Malignant Transformation

Next, we aimed to investigate the genetic and epigenetic alterations involved in malignant transformation of HCA to HCC. We observed a progressively increased chromosomal instability in borderline HCA/HCC lesions and in HCC derived from malignant transformation compared with classical HCA ($p = 0.05$; Figure 7A; Table S10). Specific loss of chromosome 6q and gain of chromosome 7 were more frequent in borderline and transformed HCA (Figure 5B). Interestingly, in methylome analysis, the intensity of the beta-value in hypomethylated genomic regions increased during malignant transformation ($p = 0.002$, ANOVA) (Figure 7B). Exome sequencing and SNP array analysis (Letouzé et al., 2010) were carried out in five cases of

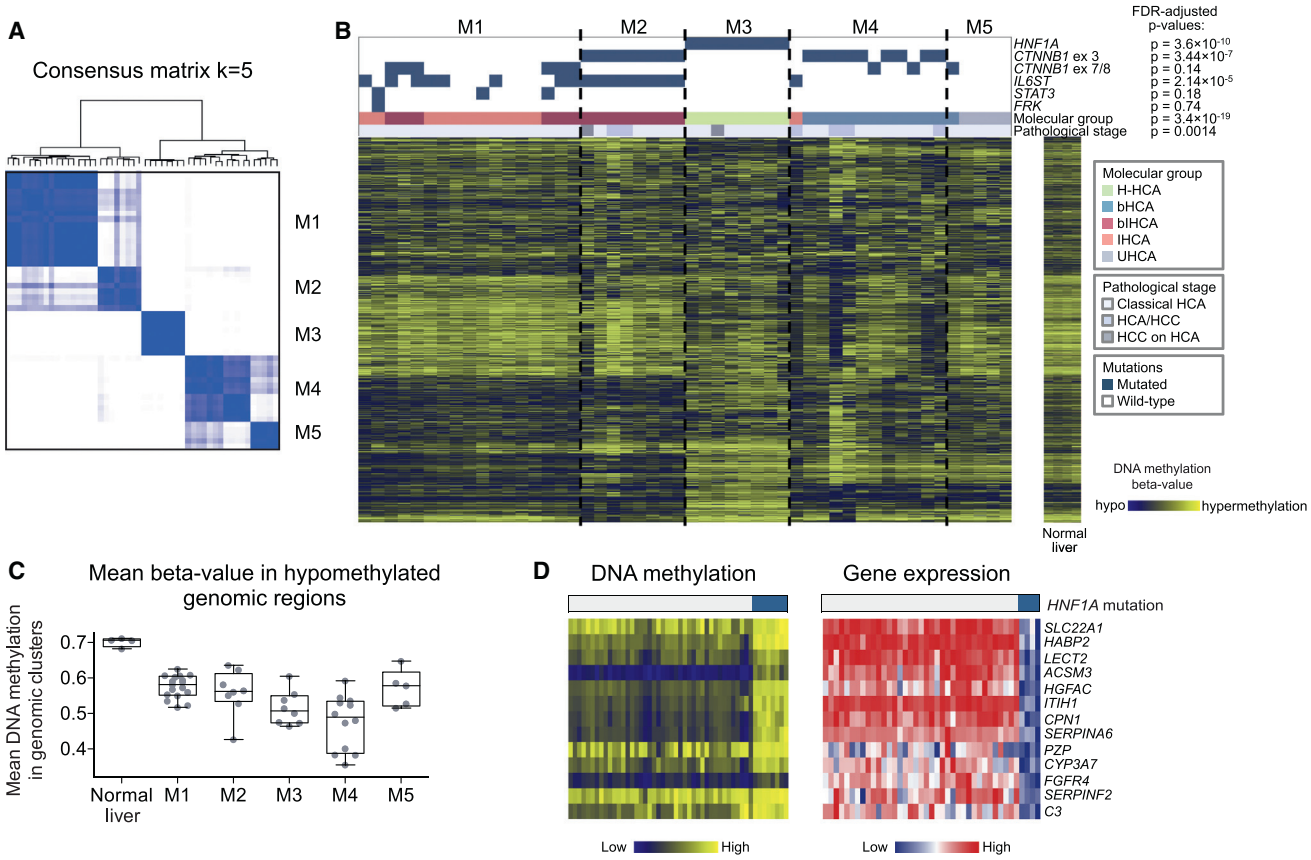

Figure 6. DNA Methylation Analysis of HCA Reveals Strong Correlation with Molecular Groups

(A) Consensus clustering analysis of 50 HCAs identifies five DNA methylation clusters.

(B) Heatmap representation of DNA methylation profiles. FDR, false discovery rate.

(C) Boxplots represent the mean DNA methylation beta-values in hypomethylated clusters in tumors of different methylation subgroups.

(D) DNA methylation and gene expression are represented for 13 liver-specific genes that are significantly hypermethylated and downregulated specifically in H-HCA.

See also Figure S4 and Tables S8 and S9.

synchronous malignant transformation for which both benign (HCA) and malignant (HCC) parts of the tumors were available. In comparison with classical HCA, the number of functional somatic mutations progressively increased in transformed HCA (mean of 24.4 events per transformed HCA, $p < 0.0001$; Figure 7C) and in malignant HCC part of the tumors (mean of 39 events per HCC counterpart) at a level similar to that observed previously in a series of classical HCC (Guichard et al., 2012) (Figures 7C and 7D). In four cases, mutations in the genes classically mutated in HCA (*CTNNB1*, *IL6ST*, and *HNF1A*) were similar in the HCA and HCC counterparts, demonstrating a common origin of the benign and transformed parts of the tumors (Figure 7G; Figure S5A). In the fifth case, the HCA and HCC parts showed different *CTNNB1* mutations, whereas 43 other mutations were found in common.

Among the other genes recurrently mutated in transformed HCA, we identified in two cases *ASH1L* (recurrently mutated in lung cancers and cell lines (Govindan et al., 2012; Liu et al., 2012) and *PEG3*, which is mutated in cholangiocarcinoma (Ong et al., 2012) (Figure S5B). A large number of private mutations were also accumulated in almost all HCA and HCC tumors, illustrating separated genetic evolution. Interestingly, in case 361, we also analyzed an HCC relapsed 3 years after the first surgical resection of a transformed HCA. Only one mutation activating β-catenin (*CTNNB1* in-frame deletion T3_A126) was common between the HCA tumor, the synchronous HCC, and the relapsed HCC. Moreover, in this patient, we identified in three different samples of nontumor liver tissues a similar T3_A126 *CTNNB1* deletion in 1/10,000 tested cells (Figure S5C). These results pointed *CTNNB1* mutation as a very early tumorigenic event in a precursor cell niche that generated three different tumors. In this case we also identified in each tumor a different mutation in the gene coding for the monoamine oxidase MAOB, suggesting that the inhibition of this gene was selected to promote the tumor development.

In the mutation screening, we added the telomerase reverse transcriptase (*TERT*) promoter, not covered in exome sequencing, because hot spot mutations were recently identified in various tumors, including HCC (Horn et al., 2013; Huang et al., 2013; Killela et al., 2013; Nault et al., 2013b). *TERT* promoter mutations were identified in five samples and in most of

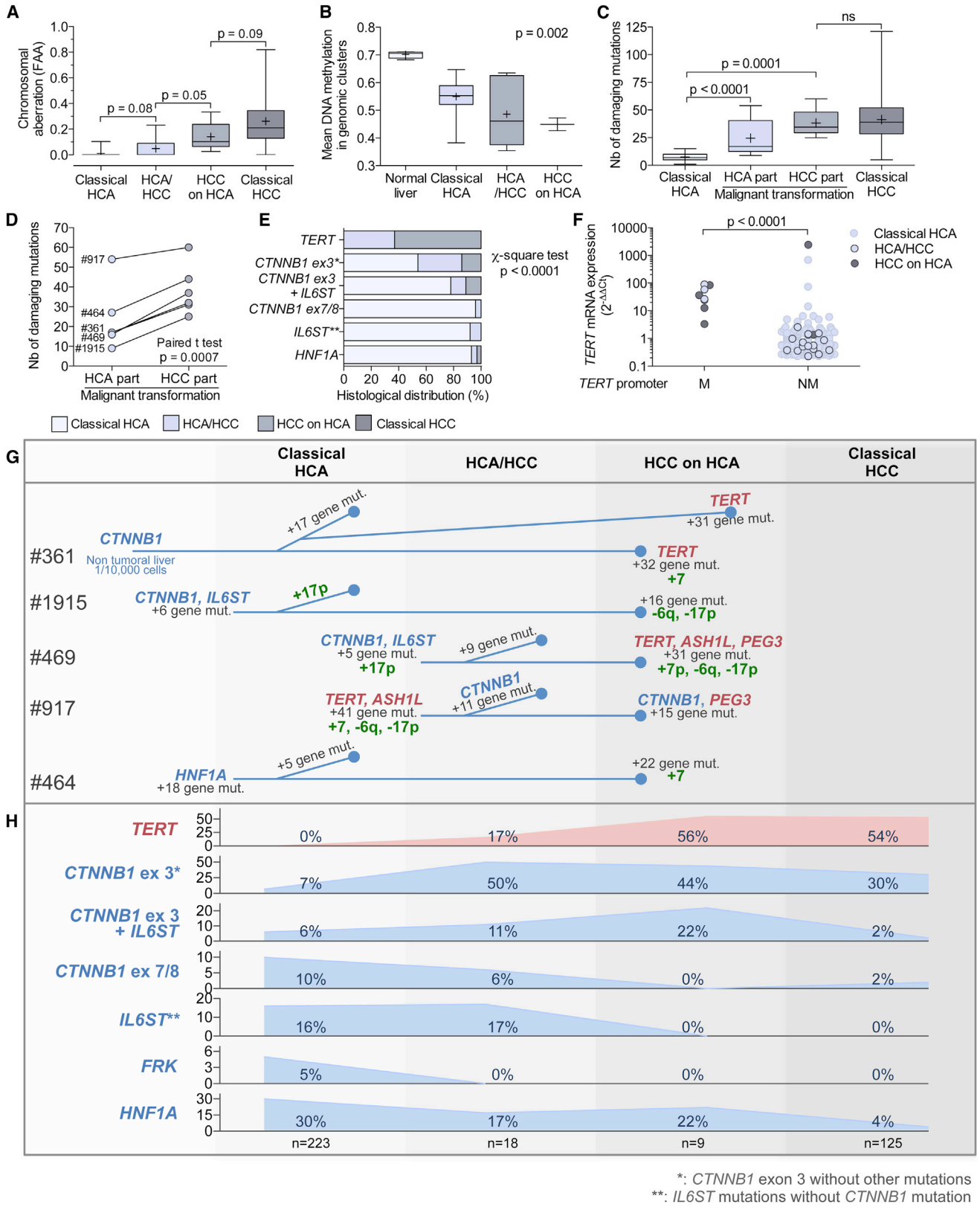

Figure 7. Time Frame of Genomic Alterations in HCA Malignant Transformation

(A) Distribution of chromosomal instability, defined as the FAA, in different pathological groups (maximum-minimum [max.-min.] boxplot, two-tailed Mann-Whitney test).

(legend continued on next page)

the cases (four of five) only in the malignant parts, suggesting that *TERT* promoter mutations could be a later oncogenic event after *CTNNB1* mutations. Then, we screened *TERT* promoter in a large series of 375 hepatocellular tumors, including 223 classical adenomas, 18 borderline lesions HCA/HCC, nine HCC derived from adenomas, and 125 classical HCC (Guichard et al., 2012). *TERT* promoter mutations were not found in classical adenomas, but they were found later in the malignant progression in borderline lesions (17%) and in transformed HCA to HCC (56%) with a frequency similar to that identified in classical HCC (54%). In HCC, *TERT* promoter mutations were significantly associated with *CTNNB1* mutations ($p < 0.0001$). Previous studies have shown that *TERT* promoter mutations create de novo consensus binding sequence for ETS/TCF transcription factors and could increase telomerase transcription (Horn et al., 2013). Here, in HCA, borderline lesion, and transformed HCA, *TERT* promoter mutations were significantly associated with an increased transcription of *TERT* ($p < 0.0001$; Figure 7F). Then, we compared the distribution of all recurrent gene mutations in the overall set of 375 tumors (Figures 7E and 7H). The proportion of *CTNNB1* exon 3 and *CTNNB1* exon 3 associated with *IL6ST* mutations progressively increased from the adenoma (13%) to the HCC-transformed lesions (66%), thus showing the significant role of these mutations in malignant progression. In contrast, the proportion of *IL6ST* alone, *CTNNB1* exon 7 and exon 8, *HNF1A*, and *FRK* mutations decreased in HCA transformed in HCC and was also lower in classical HCC, suggesting that these genes are not significantly involved in malignant transformation process.

By integrating all the omic results with the clinical and pathological features and with the identification of *FRK*, rare *JAK1*, and exon 10 *IL6ST*-activating mutations, we have enriched the mutational spectrum of inflammatory HCA, finally composed of mutations in *IL6ST* (26% of HCA), *FRK* (5%), *STAT3* (2%), *GNAS* (2%), and *JAK1* in 1% (Figure 8A). Three pathways recurrently altered in HCA (HNF1A inactivation, STAT3 or β-catenin activation alone) are associated with the benign phenotype of the tumors and specific histological features (Figure 8B). In contrast, the malignant transformation is strongly associated with characteristic gene mutations (*CTNNB1* exon 3 and *TERT* promoter mutations), chromosome alterations, and hypomethylation accumulated in time frame together with previously described specific clinical features (male sex and androgen therapy, Nault et al., 2013a; Figure 8C).

DISCUSSION

Whole-exome sequencing of hepatocellular adenomas revealed the high genetic diversity of these tumors, and the genes recurrently mutated in hepatocyte benign tumorigenesis and in the subsequent malignant transformation. In this study we identified recurrent somatic mutations of *FRK* leading to an activation of the FRK kinase activity and to constitutive STAT3 activation associated with the inflammatory phenotype of HCA. Whereas the activation of STAT3 by Src has been previously described in vitro (Bromberg et al., 1998; Turkson et al., 1998), we showed that FRK mutants induce STAT3 activation in vitro, in vivo, and in human tumors. Also, whereas FRK has been proposed as a tumor suppressor in breast cancer (Yim et al., 2009), here we demonstrated the proproliferative function of mutant FRK during benign tumorigenesis. In the liver, FRK mutants were identified only in benign tumors, whereas mouse models of gastrointestinal cancer have also demonstrated opposite functions of STAT3 at early step of tumorigenesis and during malignant transformation (Grivennikov and Karin, 2010; Lee et al., 2012; Musteanu et al., 2010). However, *FRK* was also reported as involved in a chromosome rearrangement with ETV6 in a leukemia (Hosoya et al., 2005), suggesting that this gene could be as well activated in malignant neoplasms. Also, the oncogenic properties of STAT3 constitutive activation could differ according to the cell of origin related to a malignant cell proliferation in lymphocytes (Fasan et al., 2013; Koskela et al., 2012) versus benign proliferation in hepatocytes mutated for *IL6ST* or *STAT3* (Pilati et al., 2011; Rebouissou et al., 2009). In addition, the dramatic response to the Src inhibitor dasatinib in vitro and in vivo supports FRK-activating mutations as a paradigm of a mutated gene addiction. Overall, the gene mutations identified in IHCA activate the STAT3 pathway to cause a common inflammatory phenotype within the tumors. Nowadays, inflammatory driver gene mutations remain to be identified in 18% of inflammatory HCA. Moreover, 10% of the adenomas remain unclassified and in these cases additional specific genetic or epigenetic defect remained to be identified.

Interestingly, our methylome analysis distinguished perfectly the five molecular groups of HCA, and identified genomic clusters of hypomethylation at gene family loci showing a close relationship between epigenetic changes, gene mutations, and phenotypes of the tumors. We also identified a set of liver-specific genes, hypermethylated and downregulated specifically in H-HCA. A previous report suggested that activation of HNF1A

(B) Boxplots represent the mean DNA methylation beta-values in hypomethylated clusters in tumors of different pathological stages (two-tailed Kruskal-Wallis test).
(C) Number of damaging mutations in classical HCA, in HCA transformed in HCC (HCA part) and in HCC resulting from a transformation of an adenoma (HCC part) and in 24 classical HCC(Guichard et al., 2012) (max.-min. boxplot, two-tailed Mann-Whitney test).
(D) Paired comparison of HCA and HCC counterparts of five malignant transformations (two-tailed paired t test).
(E) Distribution of the pathological groups of tumors mutated in *TERT* promoter, exon 3 of *CTNNB1* without *IL6ST* mutation, both exon 3 of *CTNNB1* and *IL6ST*, *IL6ST* without *CTNNB1* mutation, exon 7 and exon 8 of *CTNNB1*, and *HNF1A* (chi-square test).
(F) *TERT* expression in mutated and nonmutated *TERT* promoter tumors according to the different pathological stages (two-tailed Mann-Whitney test).
(G) Accumulation of genomic alterations in five malignant transformations was defined according to whole-exome sequencing and SNP array analysis. Red indicates genes recurrently mutated in transformed HCA, blue indicates genes recurrently mutated in classical HCA, and in green indicates recurrent chromosomal alterations.
(H) Frequency of mutations in *TERT* promoter, exon 3 of *CTNNB1* without *IL6ST* mutations, both exon 3 of *CTNNB1* and *IL6ST*, *IL6ST* without *CTNNB1* mutations, exon 7 and exon 8 of *CTNNB1*, and *HNF1A* according to the pathological groups.
See also Figure S5 and Table S10.

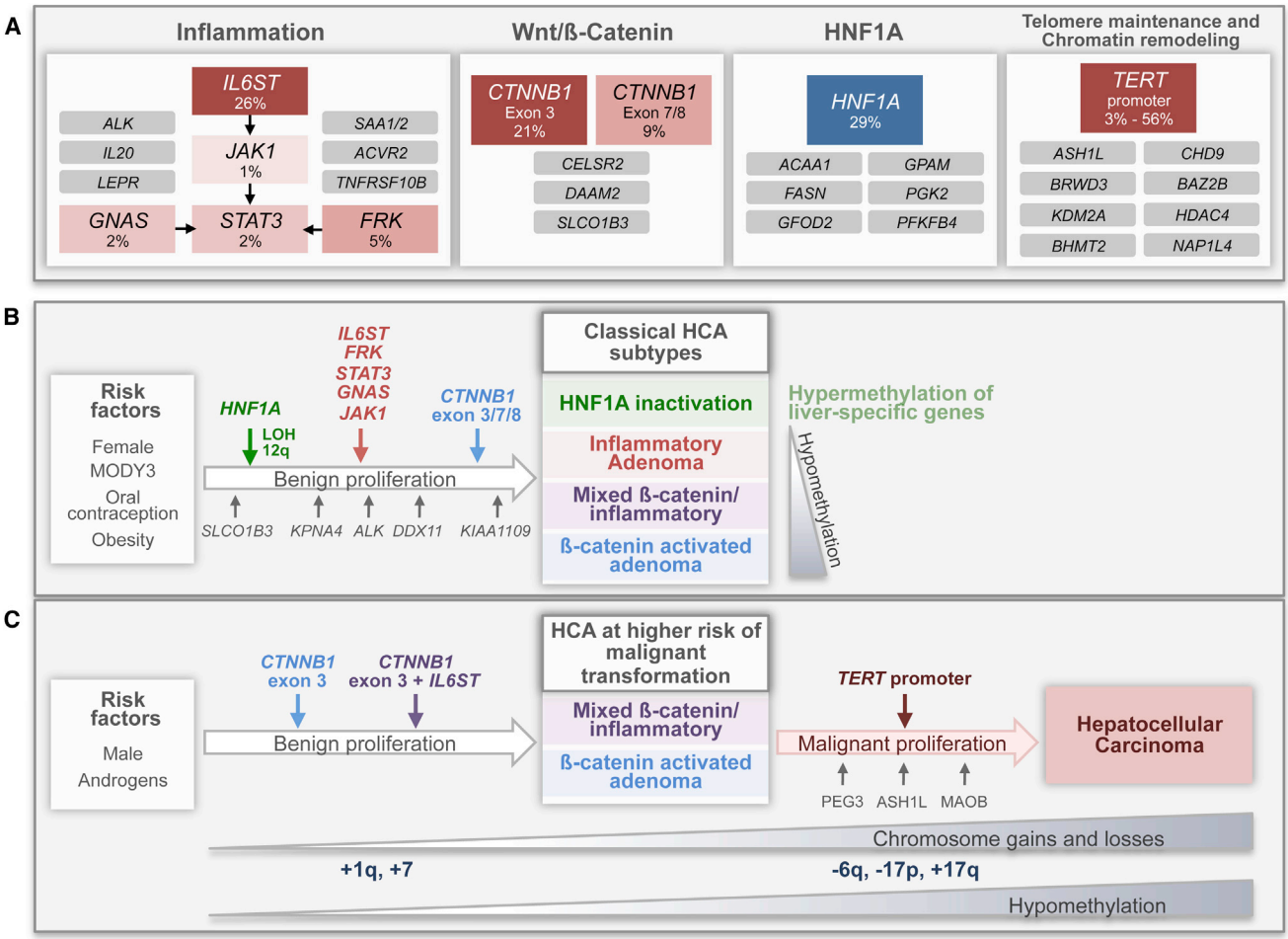

Figure 8. Genes and Pathways Implicated in HCA Initiation and Malignant Transformation

Major pathways (A) commonly altered by somatic mutations in classical HCA. Alteration frequencies are expressed as a percentage of mutation in the validation series of 250 tumors (red or blue when activated or inactivated, respectively) or 35 exome-sequenced (gray) HCAs; for unique gene mutation, no frequency is indicated. Arrows are positive interactions between two genes. Integration of the major genomic alterations occurring in classical HCA (B) and in malignant transformation of HCA in HCC (C).

target genes might involve chromatin remodeling and DNA demethylation (Pontoglio et al., 1997). Alternatively, active transcription could protect CpG islands from methylation, so hypermethylation may be a consequence of prior gene silencing (Clark and Melki, 2002). Further experiments are needed to determine whether DNA hypermethylation precedes or follows the silencing of liver-specific genes in H-HCA, but these epigenetic changes are likely to play an active role in this molecular group of HCA, and they suggest that driver genetic alterations could induce widespread epigenetic modification in hepatocellular benign tumors.

Analysis of the progression from HCA to HCC suggested that the occurrence of *CTNNB1*-activating mutation in a single cell could initiate benign liver tumorigenesis as a very early event in patient 361. However, because almost all the adenomas activated for β-catenin accumulate additional mutation in recurrent (*IL6ST*) or nonrecurrent genes, it is highly suggestive of the requirement of additional events to *CTNNB1* activating mutation to promote a benign clonal proliferation. These results are in accordance with the transgenic mouse model of hepatic *CTNNB1* mutant expression in which the constitutive Wnt pathway activation is not sufficient for hepatocarcinogenesis (Cadoret et al., 2001; Harada et al., 2002). As in other tumor types (Vogelstein et al., 1988), accumulation of chromosome aberrations is also a typical feature of malignant transformation of HCA. Here, in hepatocellular tumors, we identified somatic-activating *TERT* promoter mutations as a major event involved in the malignant transformation of hepatocellular adenomas in association with β-catenin activation. These results suggest a step-by-step model where *CTNNB1* mutations are early mutational events in benign liver tumorigenesis, although not sufficient to induce HCC in normal liver alone; telomerase reactivation through *TERT* promoter mutations is consequently required to promote full malignant transformation. Identification of *CTNNB1* and *TERT* promoter mutation as key genetic determinants of malignant transformation in HCA will be useful to propose tailored treatment in these subtypes of patients.

In conclusion, we reported a comprehensive genomic analysis of hepatocellular adenoma resulting from the benign proliferation of hepatocytes and their malignant transformation in hepatocellular carcinoma. Integrated analyses revealed the high robustness of the HCA molecular classification: all subclasses of tumors defined by the different omics are closely related together and with HCA tumor phenotypes. In addition, this classification will have clinical impact through identification of therapeutic targets and the selection of patients with high risk of malignant transformation that could require more aggressive treatment.

EXPERIMENTAL PROCEDURES

Liver Samples and Clinical Data

All tumors and corresponding nontumor liver tissues were frozen after surgical resection. These tumors were clinically and genetically characterized; they were previously included in genetic and phenotypic studies (Tables S1 and S2). The study was approved by the local Ethics Committee (Paris Saint-Louis), INSERM institutional review board in 2010, and informed consent was obtained from all subjects in accordance with French legislation. HCA were classified in (1) H-HCA according to the presence of HNF1A inactivation (73/250, 29%); (2) bHCA defined by a somatic β-catenin-activating mutation involving exon 3 and/or an overexpression of glutamine synthase and LGR5, two β-catenin target genes (53/250, 21%); and (3) IHCA defined by the presence of inflammatory infiltrates and a serum amyloid A2 and C-reactive protein overexpression (118/250, 47%); in 25 cases (10%), HCAs were both inflammatory and *CTNNB1* mutated (bIHCA). The remaining 31 cases (12%) were unclassified HCA (UHCA) when we began this study.

Genomic Analysis

Whole-exome sequencing was performed as described previously (Guichard et al., 2012). The false-positive rate of somatic mutations in WES was estimated to 2.5% after 3,000 verifications in Sanger sequencing performed in previous analyses. Comparative genomic hybridization-SNP was performed on 126 tumors with HumanCNV370-Duo v1.0 (47 tumors) or HumanOmniExpressBeadchips (79 tumors) (both from Illumina). When several samples were available from a same patient, tumor progression trees were reconstructed using the TuMult algorithm (Letouzé et al., 2010). DNA methylation profiles of 50 hepatocellular adenomas and four normal liver samples were determined using HumanMethylation450 arrays (Illumina). The ConsensusClusterPlus package (Bioconductor) was used for consensus clustering analysis. Transcriptional profiling experiments were performed using oligonucleotide GeneChips HG-U133A (Affymetrix).

Functional Analysis

FRK, *JAK1*, *IL6ST*, and *CTNNB1* mutants were obtained using the QuickChange XL site-directed mutagenesis kit (Stratagene) using primers described in Supplemental Experimental Procedures, and then used to transiently transfect Hep3B, Huh7, NIH 3T3, and Ba/F3 cells. Ba/F3- and NIH 3T3-transfected cells were selected by a treatment with Geneticin (800 and 700 μg/ml, respectively; Life Technologies). Kinase assay was performed by AlphaScreen-based assays (PerkinElmer). BALB/c-nu/nu mice used for xenograft experiments were housed in the pathogen-free animal facility at the Institut Universitaire d'Hématologie, Paris. All experimental procedures were done in compliance with the French Ministry of Agriculture regulations for animal experimentation.

A complete description of the materials and methods is provided in Supplemental Experimental Procedures.

ACCESSION NUMBERS

Sequencing data are accessible at European Genome-phenome Archive (http://www.ebi.ac.uk/ega/) under accession number EGAS00001000679. All variants and tumor features are deposited in the International Cancer Genome Consortium (ICGC) portal (ftp://data.dcc.icgc.org/version_9/). SNP array and DNA methylation data are available from Gene Expression Omnibus as accession number GSE43273.

SUPPLEMENTAL INFORMATION

Supplemental Information includes Supplemental Experimental Procedures, five figures, and ten tables and can be found with this article online at http://dx.doi.org/10.1016/j.ccr.2014.03.005.

AUTHOR CONTRIBUTIONS

C.P., S.I., E.L., J.-C.N., and A.B. designed, analyzed, and verified the genomic data; C.P., K.P., A.F., S.T., and F. Canal designed and performed the functional analyses; S.I. and E.L. performed statistical analyses; C.P., A.B., G.M., J.-C.N., M.M., and G.C. performed the sequencing validation; J.C., C.B., V.P., B.T., J.-Y.S., A.d.M., C.G., and P.B.-S. provided samples, pathological reviewing, and clinical information; J.C., K.P., and P.B.-S. performed immunohistochemical analyses; E.C. and F. Calvo participated to the achievement of the study; J.Z.-R. designed and coordinated the overall study; and all the authors contributed to writing the manuscript.

ACKNOWLEDGMENTS

We warmly thank Isabelle Desitter, Cécile Guichard, and Ichrafe Ben Maad for helpful participation in this work. We also thank Jean Saric, Christophe Laurent, Brigitte Le Bail, Anne Rullier, Laurence Chiche (CHU Bordeaux) and Jeanne Tran Van Nhieu, Daniel Cherqui, Daniel Azoulay (CHU Henri Mondor, Créteil), and the tumor bank of CHU Bordeaux and CHU Henri Mondor for contributing to the tissue collection. We thank Randall Moon (Howard Hughes Medical Institute, University of Washington) and Eric Fearon (Regents of the University of Michigan) who provided the plasmids. This work was supported by the INCa within the ICGC project and 2010-1-PL BIO-02-1, the Ligue Nationale Contre le Cancer ("Carte d'identité des tumeurs" program), the Association pour la recherche contre le Cancer, ARC (grant 3194), and the Réseau national CRB Foie and BioIntelligence (OSEO). C.P. was supported by a fellowship from MENRT and ARC and J.-C.N. was supported by a fellowship from Inca.

Received: July 10, 2013
Revised: November 14, 2013
Accepted: March 4, 2014
Published: April 14, 2014

REFERENCES

Acevedo, L.G., Bieda, M., Green, R., and Farnham, P.J. (2008). Analysis of the mechanisms mediating tumor-specific changes in gene expression in human liver tumors. Cancer Res. *68*, 2641–2651.

Bacq, Y., Jacquemin, E., Balabaud, C., Jeannot, E., Scotto, B., Branchereau, S., Laurent, C., Bourlier, P., Pariente, D., de Muret, A., et al. (2003). Familial liver adenomatosis associated with hepatocyte nuclear factor 1alpha inactivation. Gastroenterology *125*, 1470–1475.

Bioulac-Sage, P., Rebouissou, S., Thomas, C., Blanc, J.F., Saric, J., Sa Cunha, A., Rullier, A., Cubel, G., Couchy, G., Imbeaud, S., et al. (2007). Hepatocellular adenoma subtype classification using molecular markers and immunohistochemistry. Hepatology *46*, 740–748.

Bioulac-Sage, P., Laumonier, H., Couchy, G., Le Bail, B., Sa Cunha, A., Rullier, A., Laurent, C., Blanc, J.F., Cubel, G., Trillaud, H., et al. (2009). Hepatocellular adenoma management and phenotypic classification: the Bordeaux experience. Hepatology *50*, 481–489.

Bluteau, O., Jeannot, E., Bioulac-Sage, P., Marqués, J.M., Blanc, J.F., Bui, H., Beaudoin, J.C., Franco, D., Balabaud, C., Laurent-Puig, P., and Zucman-Rossi, J. (2002). Bi-allelic inactivation of TCF1 in hepatic adenomas. Nat. Genet. *32*, 312–315.

Bromberg, J.F., Horvath, C.M., Besser, D., Lathem, W.W., and Darnell, J.E., Jr. (1998). Stat3 activation is required for cellular transformation by v-src. Mol. Cell. Biol. *18*, 2553–2558.

Cadoret, A., Ovejero, C., Saadi-Kheddouci, S., Souil, E., Fabre, M., Romagnolo, B., Kahn, A., and Perret, C. (2001). Hepatomegaly in transgenic mice expressing an oncogenic form of beta-catenin. Cancer Res. *61*, 3245–3249.

Calderaro, J., Labrune, P., Morcrette, G., Rebouissou, S., Franco, D., Prévot, S., Quaglia, A., Bedossa, P., Libbrecht, L., Terracciano, L., et al. (2013). Molecular characterization of hepatocellular adenomas developed in patients with glycogen storage disease type I. J. Hepatol. *58*, 350–357.

Chen, Y.J., Chen, P.J., Lee, M.C., Yeh, S.H., Hsu, M.T., and Lin, C.H. (2002). Chromosomal analysis of hepatic adenoma and focal nodular hyperplasia by comparative genomic hybridization. Genes Chromosomes Cancer *35*, 138–143.

Clark, S.J., and Melki, J. (2002). DNA methylation and gene silencing in cancer: which is the guilty party? Oncogene *21*, 5380–5387.

Fasan, A., Kern, W., Grossmann, V., Haferlach, C., Haferlach, T., and Schnittger, S. (2013). STAT3 mutations are highly specific for large granular lymphocytic leukemia. Leukemia *27*, 1598–1600.

Flex, E., Petrangeli, V., Stella, L., Chiaretti, S., Hornakova, T., Knoops, L., Ariola, C., Fodale, V., Clappier, E., Paoloni, F., et al. (2008). Somatically acquired JAK1 mutations in adult acute lymphoblastic leukemia. J. Exp. Med. *205*, 751–758.

Govindan, R., Ding, L., Griffith, M., Subramanian, J., Dees, N.D., Kanchi, K.L., Maher, C.A., Fulton, R., Fulton, L., Wallis, J., et al. (2012). Genomic landscape of non-small cell lung cancer in smokers and never-smokers. Cell *150*, 1121–1134.

Grivennikov, S.I., and Karin, M. (2010). Inflammation and oncogenesis: a vicious connection. Curr. Opin. Genet. Dev. *20*, 65–71.

Guichard, C., Amaddeo, G., Imbeaud, S., Ladeiro, Y., Pelletier, L., Maad, I.B., Calderaro, J., Bioulac-Sage, P., Letexier, M., Degos, F., et al. (2012). Integrated analysis of somatic mutations and focal copy-number changes identifies key genes and pathways in hepatocellular carcinoma. Nat. Genet. *44*, 694–698.

Harada, N., Miyoshi, H., Murai, N., Oshima, H., Tamai, Y., Oshima, M., and Taketo, M.M. (2002). Lack of tumorigenesis in the mouse liver after adenovirus-mediated expression of a dominant stable mutant of beta-catenin. Cancer Res. *62*, 1971–1977.

Horn, S., Figl, A., Rachakonda, P.S., Fischer, C., Sucker, A., Gast, A., Kadel, S., Moll, I., Nagore, E., Hemminki, K., et al. (2013). TERT promoter mutations in familial and sporadic melanoma. Science *339*, 959–961.

Hosoya, N., Qiao, Y., Hangaishi, A., Wang, L., Nannya, Y., Sanada, M., Kurokawa, M., Chiba, S., Hirai, H., and Ogawa, S. (2005). Identification of a SRC-like tyrosine kinase gene, FRK, fused with ETV6 in a patient with acute myelogenous leukemia carrying a t(6;12)(q21;p13) translocation. Genes Chromosomes Cancer *42*, 269–279.

Huang, F.W., Hodis, E., Xu, M.J., Kryukov, G.V., Chin, L., and Garraway, L.A. (2013). Highly recurrent TERT promoter mutations in human melanoma. Science *339*, 957–959.

Jeannot, E., Mellottee, L., Bioulac-Sage, P., Balabaud, C., Scoazec, J.Y., Tran Van Nhieu, J., Bacq, Y., Michalak, S., Buob, D., Laurent-Puig, P., et al.; Groupe d'étude Génétique des Tumeurs Hépatiques (INSERM Network) (2010). Spectrum of HNF1A somatic mutations in hepatocellular adenoma differs from that in patients with MODY3 and suggests genotoxic damage. Diabetes *59*, 1836–1844.

Killela, P.J., Reitman, Z.J., Jiao, Y., Bettegowda, C., Agrawal, N., Diaz, L.A., Jr., Friedman, A.H., Friedman, H., Gallia, G.L., Giovanella, B.C., et al. (2013). TERT promoter mutations occur frequently in gliomas and a subset of tumors derived from cells with low rates of self-renewal. Proc. Natl. Acad. Sci. USA *110*, 6021–6026.

Koskela, H.L., Eldfors, S., Ellonen, P., van Adrichem, A.J., Kuusanmäki, H., Andersson, E.I., Lagström, S., Clemente, M.J., Olson, T., Jalkanen, S.E., et al. (2012). Somatic STAT3 mutations in large granular lymphocytic leukemia. N. Engl. J. Med. *366*, 1905–1913.

Laumonier, H., Bioulac-Sage, P., Laurent, C., Zucman-Rossi, J., Balabaud, C., and Trillaud, H. (2008). Hepatocellular adenomas: magnetic resonance imaging features as a function of molecular pathological classification. Hepatology *48*, 808–818.

Lee, J., Kim, J.C., Lee, S.E., Quinley, C., Kim, H., Herdman, S., Corr, M., and Raz, E. (2012). Signal transducer and activator of transcription 3 (STAT3) protein suppresses adenoma-to-carcinoma transition in Apcmin/+ mice via regulation of Snail-1 (SNAI) protein stability. J. Biol. Chem. *287*, 18182–18189.

Letouzé, E., Allory, Y., Bollet, M.A., Radvanyi, F., and Guyon, F. (2010). Analysis of the copy number profiles of several tumor samples from the same patient reveals the successive steps in tumorigenesis. Genome Biol. *11*, R76.

Liu, J., Lee, W., Jiang, Z., Chen, Z., Jhunjhunwala, S., Haverty, P.M., Gnad, F., Guan, Y., Gilbert, H.N., Stinson, J., et al. (2012). Genome and transcriptome sequencing of lung cancers reveal diverse mutational and splicing events. Genome Res. *22*, 2315–2327.

Musteanu, M., Blaas, L., Mair, M., Schlederer, M., Bilban, M., Tauber, S., Esterbauer, H., Mueller, M., Casanova, E., Kenner, L., et al. (2010). Stat3 is a negative regulator of intestinal tumor progression in Apc(Min) mice. Gastroenterology *138*, 1003–1011.

Nault, J.C., Fabre, M., Couchy, G., Pilati, C., Jeannot, E., Tran Van Nhieu, J., Saint-Paul, M.C., De Muret, A., Redon, M.J., Buffet, C., et al. (2012). GNAS-activating mutations define a rare subgroup of inflammatory liver tumors characterized by STAT3 activation. J. Hepatol. *56*, 184–191.

Nault, J.C., Bioulac-Sage, P., and Zucman-Rossi, J. (2013a). Hepatocellular benign tumors-from molecular classification to personalized clinical care. Gastroenterology *144*, 888–902.

Nault, J.C., Mallet, M., Pilati, C., Calderaro, J., Bioulac-Sage, P., Laurent, C., Laurent, A., Cherqui, D., Balabaud, C., and Zucman-Rossi, J. (2013b). High frequency of telomerase reverse-transcriptase promoter somatic mutations in hepatocellular carcinoma and preneoplastic lesions. Nat. Commun. *4*, 2218.

Ong, C.K., Subimerb, C., Pairojkul, C., Wongkham, S., Cutcutache, I., Yu, W., McPherson, J.R., Allen, G.E., Ng, C.C., Wong, B.H., et al. (2012). Exome sequencing of liver fluke-associated cholangiocarcinoma. Nat. Genet. *44*, 690–693.

Pilati, C., Amessou, M., Bihl, M.P., Balabaud, C., Nhieu, J.T., Paradis, V., Nault, J.C., Izard, T., Bioulac-Sage, P., Couchy, G., et al. (2011). Somatic mutations activating STAT3 in human inflammatory hepatocellular adenomas. J. Exp. Med. *208*, 1359–1366.

Pontoglio, M., Faust, D.M., Doyen, A., Yaniv, M., and Weiss, M.C. (1997). Hepatocyte nuclear factor 1alpha gene inactivation impairs chromatin remodeling and demethylation of the phenylalanine hydroxylase gene. Mol. Cell. Biol. *17*, 4948–4956.

Poussin, K., Pilati, C., Couchy, G., Calderaro, J., Bioulac-Sage, P., Bacq, Y., Paradis, V., Leteurtre, E., Sturm, N., Ramos, J., et al. (2013). Biochemical and functional analyses of gp130 mutants unveil JAK1 as a novel therapeutic target in human inflammatory hepatocellular adenoma. Oncoimmunology *2*, e27090.

Rebouissou, S., Amessou, M., Couchy, G., Poussin, K., Imbeaud, S., Pilati, C., Izard, T., Balabaud, C., Bioulac-Sage, P., and Zucman-Rossi, J. (2009). Frequent in-frame somatic deletions activate gp130 in inflammatory hepatocellular tumours. Nature *457*, 200–204.

Rooks, J.B., Ory, H.W., Ishak, K.G., Strauss, L.T., Greenspan, J.R., Hill, A.P., and Tyler, C.W., Jr. (1979). Epidemiology of hepatocellular adenoma. The role of oral contraceptive use. J. Am. Med. Assoc. *242*, 644–648.

Staerk, J., Kallin, A., Demoulin, J.B., Vainchenker, W., and Constantinescu, S.N. (2005). JAK1 and Tyk2 activation by the homologous polycythemia vera JAK2 V617F mutation: cross-talk with IGF1 receptor. J. Biol. Chem. *280*, 41893–41899.

Stefanska, B., Huang, J., Bhattacharyya, B., Suderman, M., Hallett, M., Han, Z.G., and Szyf, M. (2011). Definition of the landscape of promoter DNA hypomethylation in liver cancer. Cancer Res. *71*, 5891–5903.

Talpaz, M., Shah, N.P., Kantarjian, H., Donato, N., Nicoll, J., Paquette, R., Cortes, J., O'Brien, S., Nicaise, C., Bleickardt, E., et al. (2006). Dasatinib in imatinib-resistant Philadelphia chromosome-positive leukemias. N. Engl. J. Med. *354*, 2531–2541.

Turkson, J., Bowman, T., Garcia, R., Caldenhoven, E., De Groot, R.P., and Jove, R. (1998). Stat3 activation by Src induces specific gene regulation and is required for cell transformation. Mol. Cell. Biol. *18*, 2545–2552.

Vogelstein, B., Fearon, E.R., Hamilton, S.R., Kern, S.E., Preisinger, A.C., Leppert, M., Nakamura, Y., White, R., Smits, A.M., and Bos, J.L. (1988). Genetic alterations during colorectal-tumor development. N. Engl. J. Med. *319*, 525–532.

Yim, E.K., Peng, G., Dai, H., Hu, R., Li, K., Lu, Y., Mills, G.B., Meric-Bernstam, F., Hennessy, B.T., Craven, R.J., and Lin, S.Y. (2009). Rak functions as a tumor suppressor by regulating PTEN protein stability and function. Cancer Cell *15*, 304–314.

Zhang, J., Ding, L., Holmfeldt, L., Wu, G., Heatley, S.L., Payne-Turner, D., Easton, J., Chen, X., Wang, J., Rusch, M., et al. (2012). The genetic basis of early T-cell precursor acute lymphoblastic leukaemia. Nature *481*, 157–163.

Zucman-Rossi, J., Jeannot, E., Nhieu, J.T., Scoazec, J.Y., Guettier, C., Rebouissou, S., Bacq, Y., Leteurtre, E., Paradis, V., Michalak, S., et al. (2006). Genotype-phenotype correlation in hepatocellular adenoma: new classification and relationship with HCC. Hepatology *43*, 515–524.